

# The Effect of Additional Severe Plastic Deformation at Elevated Temperatures on the Microstructure and Functional Properties of the Ultrafine-Grained Al–0.4Zr Alloy

T. S. Orlova<sup>a, \*</sup>, T. A. Latynina<sup>b</sup>, M. Yu. Murashkin<sup>c, d</sup>, and V. U. Kazykhanov<sup>d</sup>

<sup>a</sup> Ioffe Institute, St. Petersburg, Russia

<sup>b</sup> St. Petersburg National Research University of Information Technologies, Mechanics and Optics, St. Petersburg, Russia

<sup>c</sup> St. Petersburg State University, St. Petersburg, Russia

<sup>d</sup> Ufa State Aviation Technical University, Institute of Advanced Materials Physics, Ufa, Russia

\*e-mail: orlova.t@mail.ioffe.ru

Received July 23, 2019; revised July 23, 2019; accepted July 24, 2019

**Abstract**—The effect of severe plastic torsion deformation (SPTD) at elevated temperatures of 230 and 280°C on the microstructure, mechanical properties, and electrical conductivity of ultrafine-grained (UFG) Al–0.4Zr alloy samples is studied. The initial UFG structure in the material under study is preliminarily appeared in the SPTD process at ambient temperatures. It is shown that simultaneous significant increases in the strength from 140 to 230–280 MPa and in the electrical conductivity from about 47.5% to 52–54% IACS take place as a result of additional deformation of the UFG Al–0.4Zr alloy at elevated temperatures. The results are compared with the effect that annealing at the same temperatures exerts on the microstructure and properties of the UFG Al–0.4Zr alloy. It is established that severe plastic deformation at comparable temperatures leads to a more efficient, compared to annealing, formation of nanoscale precipitates of the Al<sub>3</sub>Zr secondary phase and, consequently, to a larger decrease in the concentration of Zr in the solid solution, which ensures a significant increase in the electrical conductivity. Based on the obtained parameters of the microstructure, the contributions of various strengthening mechanisms to the general strengthening and electron scattering mechanisms to the electrical resistance are estimated. An comparative analysis of theoretical estimates with experimental results indicates that the strengthening in the UFG structure of the Al–0.4Zr alloy that is caused by additional SPD at elevated temperatures cannot be described by the action of only strengthening mechanisms traditional for UFG materials. Possible reasons for the obtained colossal strengthening are discussed.

**Keywords:** ultrafine-grained aluminum alloy, severe plastic deformation, microstructure, strength, electrical conductivity, strengthening mechanisms

**DOI:** 10.1134/S1063783419120357

## 1. INTRODUCTION

The creation of a microstructural design that provides a significant increase in the functional properties of metals and alloys is among the most effective approaches to modern physical science of materials. It is known that the use of the methods of severe plastic deformation (SPD), leading to significant grain refinement, can significantly increase the strength of a number of metals and alloys [1–6]. However, SPD leads to an increase in the density of defects in the crystal structure (dislocation density, grain boundaries, etc.), which negatively affects the value of electrical conductivity. Therefore, the production of conductive aluminum alloys that show simultaneously a high strength and electrical conductivity, as well as increased thermal stability of mechanical properties at temperatures up to 200°C is a topical problem. For

increasing the thermal stability of mechanical properties, Zr added in a concentration of 0.2–0.5 wt % is an important dopant [7, 8].

Moreover, as has recently been shown for the Al–0.4Zr alloy (wt %) with the ultrafine-grained (UFG) structure obtained by the method of severe plastic torsion deformation (SPTD), significant additional strengthening is observed as a result of low-temperature annealing at temperatures  $T_{AN} = 90–280^{\circ}\text{C}$  with the maximum of strengthening (up to about 65%) at  $T_{AN} = 230^{\circ}\text{C}$  [9]. It should be noted that Zr was mainly in a solid solution both in the initial state obtained by the method of combined casting and rolling, and in the state after SPTD [10, 11]. In the range of annealing temperatures of  $T_{AN} = 90–150^{\circ}\text{C}$ , the strengthening effect for the UFG Al–0.4Zr alloy was qualitatively and quantitatively similar to that observed previously

in technically pure Al [12]. With an increase in the annealing temperature to  $T_{AN} = 230^{\circ}\text{C}$ , further strengthening of the UFG alloy was observed, which is accompanied by a decrease in the electrical resistivity and a corresponding increase in the electrical conductivity from 47.4 to 48.7% IACS (the electrical conductivity is given in International Annealed Copper Standard units). An increase in the electrical conductivity is caused by a decrease in the concentration of Zr in the solid solution as a result of the formation of nanosized particles of the secondary  $\text{Al}_3\text{Zr}$  phase. However, the colossal effect of strengthening with annealing cannot be explained by dispersion strengthening, as was shown in [9].

It is well known that deformation of aluminum alloys at elevated temperatures can lead to processes of deformation aging (DA) in them, which contributes to the formation of nanosized particles of intermetallic phases, as a rule, more efficiently than annealing at identical temperatures. For example, it was shown for the UFG Al–2Fe alloy [13] structured by severe plastic deformation at room temperature (RT) that the use of additional SPD at elevated temperatures leads to a significantly higher electrical conductivity at the same level of strength when compared to the use of annealing at the same temperature. The efficiency of using additional SPD at elevated temperatures for a deeper decomposition of the solid solution and the formation of nanosized particles of the secondary phases as a result of DA, which ensured a significant increase in the electrical conductivity while maintaining a relatively high level of strength, was also shown for an alloy of the Al–Mg–Si system in the UFG state [1].

In this work, the effect of DA implemented by SPTD at elevated temperatures on the microstructure, mechanical properties, and electrical conductivity of the Al–0.4Zr alloy in the UFG state formed by preliminary SPTD processing at RT is studied. The obtained results are compared with the data obtained earlier [9] when studying the effect of annealing on the microstructure and properties of the UFG Al–0.4Zr alloy, which we partially supplemented in this work.

## 2. MATERIALS AND TECHNIQUES

Samples of the initial Al–0.4Zr alloy (wt %) with a chemical composition of 99.25 Al, 0.393 Zr, 0.023 Si, 0.242 Fe, 0.018 Zn, 0.026 V, and 0.05 wt % the rest elements were obtained by the method of combined casting and rolling in the RUSAL company (Moscow, Russia) [14, 15]. In the initial state, Zr atoms are predominantly in a solid solution in the aluminum matrix [10, 11]. Billets in the form of cylinders with a diameter of 9.5 mm and a height of 8 mm were cut from the initial bar and processed by the SPTD method at a hydrostatic pressure of 6 GPa in 10 revolutions at RT [16, 17]. As a result of this treatment, disk-shaped samples with a diameter of 20 mm and a thickness of

1.2 mm were obtained. The true strain at a distance of 5 mm from the center of the disk was  $\gamma \approx 6.6$  [17]. Hereinafter, samples processed by SPTD at RT are designated as HPT\_RT (high-pressure torsion\_room temperature). Some of the samples after SPTD at RT were processed by SPTD under a pressure of 6 GPa at elevated temperatures of  $T_{HPT} = 230$  and  $280^{\circ}\text{C}$  in  $n = 1, 5, 10,$  and  $20$  revolutions. Hereinafter, samples after two stages of SPTD at different temperatures are designated as HPT\_RT–HPT\_ $T_{HPT}$ \_ $n$ . The choice of temperatures of  $T_{HPT} = 230$  and  $280^{\circ}\text{C}$  was determined by the fact that the maximum annealing strengthening upon annealing of the HPT\_RT samples for 1 h was observed at an annealing temperature of  $T_{AN} = 230^{\circ}\text{C}$ , while  $T_{AN} = 280^{\circ}\text{C}$  corresponded to the end of the temperature range in which the strengthening with annealing was observed [9]. To carry out a series of additional investigations of the effect of annealing, several samples after SPTD at RT were annealed at a temperature of  $230^{\circ}\text{C}$  for 1 and 5 h in the same way as was done in [9]. Hereinafter, these samples are designated as HPT\_RT–AN\_ $T_{AN}$ .

The microstructure of the samples was studied by the X-ray diffraction (XRD), electron backscatter diffraction (EBSD), and transmission electron microscopy (TEM) methods. An X-ray structure analysis was performed on a Bruker D8 DISCOVER diffractometer in the standard mode of symmetric  $\phi$ – $2\theta$  scanning. Based on the obtained X-ray diffraction patterns, lattice parameter  $a$ , the mean size of coherent scattering domains (DXRD), and the level of microdistortions ( $\langle \epsilon^2 \rangle^{1/2}$ ) were determined by the Pauli method using the TOPAS5.0 software package. The density of dislocations ( $L_{dis}$ ) was calculated as follows [18]:

$$L_{dis} = \frac{2\sqrt{3} \langle \epsilon^2 \rangle^{1/2}}{D_{XRD} b}, \quad (1)$$

where  $b = 2.86 \text{ \AA}$  is the Burgers vector.

The EBSD studies were performed on a Zeiss Merlin scanning electron microscope in the region of about  $1200 \mu\text{m}^2$  with a scanning step of  $0.2 \mu\text{m}$ ; more than 1000 grains were analyzed for each state. Using the EBSD maps, the size distributions of grains and the angular distribution of grain boundaries (GBs) were determined from the misalignment angle ( $\theta$ ). The averaged grain size ( $d_{av}$ ) was determined by the method of grain reconstruction [19]. From the obtained data, the averaged misalignment angle ( $\theta_{av}$ ) of GBs and the fraction of high-angle grain boundaries (HAGBs) with a misalignment angle of  $\theta \geq 15^{\circ}$  ( $f_{\geq 15}$ ) were also determined from the obtained data.

Electron microscopic studies were performed on a JEOLJEM2100 electron microscope. Thin foils for TEM studies were prepared by mechanical polishing followed by two-jet electrochemical polishing in the mode described in [12].

Mechanical properties were studied by measuring the microhardness and uniaxial tension. The Vickers microhardness was measured using a Shimadzu HMV-G microhardness tester with an applied load of 1 N for 15 s. Each sample was measured at least 15 times.

Uniaxial tensile tests were carried out on a Shimadzu AG-XD Plus testing machine with a constant deformation rate of  $5 \times 10^{-4} \text{ s}^{-1}$ . For this, samples in the form of a blade with a working part width of 2 mm and a working part length of 6 mm were cut. The cutting scheme and configuration of the samples are described in [9]. The sample deformation was recorded using a TRViewX55S video extensometer. For each state, at least three samples were tested.

Electrical conductivity  $\sigma_{RT}$  of the alloy at RT was measured using a VE-27NTs/4-5 eddy current tester with a relative error of  $\pm 2\%$  according to Russian State standard GOST 27333-87. In addition, resistivity  $\rho_{77}$  at 77 K was measured using the standard four-point method. The error in the measurement of electrical resistivity was  $< 2\%$ . The temperature of the sample was controlled by a silicon diode with an accuracy of  $\pm 0.03 \text{ K}$ . In more detail, the measurement of electrical resistivity by the four-point method is described in [12].

### 3. EXPERIMENTAL RESULTS

#### 3.1. Choice of Additional SPTD Parameters at Elevated Temperatures

Figure 1a shows the dependences of the microhardness ( $H_V$ ) of the Al–0.4Zr alloy in the HPT\_RT state on the number of revolutions during the additional SPTD at  $T_{\text{HPT}} = 230^\circ\text{C}$  (curve 1) and  $280^\circ\text{C}$  (curve 2). The microhardness values in the initial state before SPTD at RT are also given in Fig. 1. As can be seen, SPTD at RT significantly increases the microhardness, as has been noted earlier in [9]. The subsequent SPTD at  $T_{\text{HPT}} = 230^\circ\text{C}$  leads to a further significant increase in  $H_V$  to a value of 820 MPa just after the first torsion revolution, but the spread of the microhardness values over the working region of the sample in this case is quite significant (Fig. 1a), which is most likely due to that a sufficiently homogeneous structure has not yet been formed after one revolution. With an increase in the number of revolutions to  $n = 10$ , the average microhardness remains at the level of  $H_V = 766 \text{ MPa}$ , and the spread of the values across the sample becomes insignificant. As  $n$  increases to 20 revolutions, the average  $H_V$  value is maintained. In the case of additional SPTD at  $T_{\text{HPT}} = 280^\circ\text{C}$ , the  $H_V$  value first increases and passes through a maximum at  $n = 1$  and then decreases almost linearly with an increase in the number of revolutions to  $n = 10$ . The resistivity decreases with an increase in the number of revolutions during the additional SPTD for both tempera-

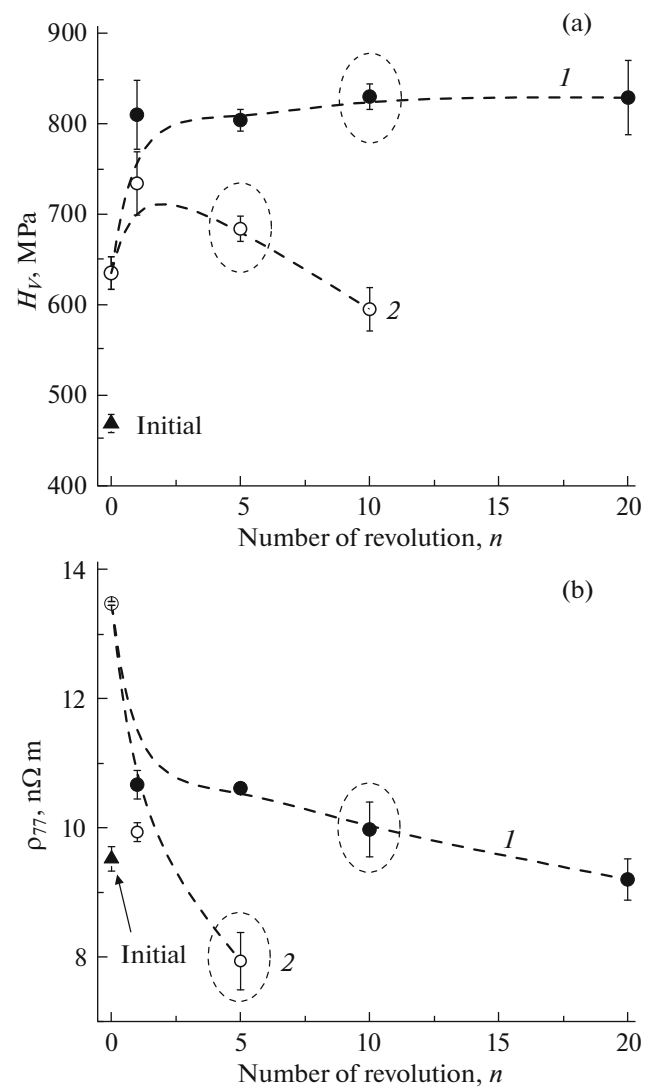


**Fig. 1.** Dependences of the (a) microhardness and (b) electrical resistivity at 77 K for the UFG Al–0.4Zr alloy (HPT\_RT) on the number of revolutions during the additional SPTD at elevated temperatures of 230 (curves 1) and  $280^\circ\text{C}$  (curves 2). The  $H_V$  and  $\rho_{77}$  values are also given for the initial state.

tures of  $T_{\text{HPT}} = 230$  and  $280^\circ\text{C}$  (Fig. 1b). To determine the effect of the number of revolutions on the resistivity, we chose resistivity measurements at 77 K, since the influence of thermal vibrations of the lattice and thermal fluctuations on the electrical resistance is reduced at low temperatures, and therefore, the relative effect of microstructural components is more pronounced. For further studies, we selected the following states with an optimal combination of strength properties (microhardness) and electrical conductivity (electrical resistivity): HPT\_RT–HPT\_230\_10 and HPT\_RT–HPT\_280\_5, further designated as HPT\_RT–HPT\_230 and HPT\_RT–HPT\_280, respectively (states that are denoted by circles in Fig. 1).

**Table 1.** EBSD and XRD data for the studied states of the Al–Zr alloy

Treatment	EBSD			XRD				Ref.
	$d_{av}$ , nm	$f_{\geq 15}$ , %	$\theta_{\geq 15}$ , deg	$\langle \epsilon^2 \rangle^{1/2}$ , %	$D_{XRD}$ , nm	$a$ , Å	$L_{dis}$ , m <sup>-2</sup>	
Initial	Length 1790 ± 20 Width 1040 ± 10	25	11.5	0.003 ± 0.0001	250 ± 5	4.0514 ± 0.0001	1.4 × 10 <sup>13</sup>	[9]
HPT_RT	835 ± 13	82	33.8	0.063 ± 0.0006	210 ± 10	4.0515 ± 0.0001	3.6 × 10 <sup>13</sup>	This study
HPT_RT–HPT_230	920 ± 15	88	36.2	0.036 ± 0.0007	480 ± 5	4.0512 ± 0.0001	9.0 × 10 <sup>12</sup>	
HPT_RT–HPT_280	925 ± 15	89	36.5	0.022 ± 0.0002	560 ± 25	4.0514 ± 0.0001	4.8 × 10 <sup>12</sup>	
HPT_RT–AN_230	880 ± 15	86	39.8	0.0300 ± 0.0001	505 ± 10	4.0516 ± 0.0001	7.2 × 10 <sup>12</sup>	[9]

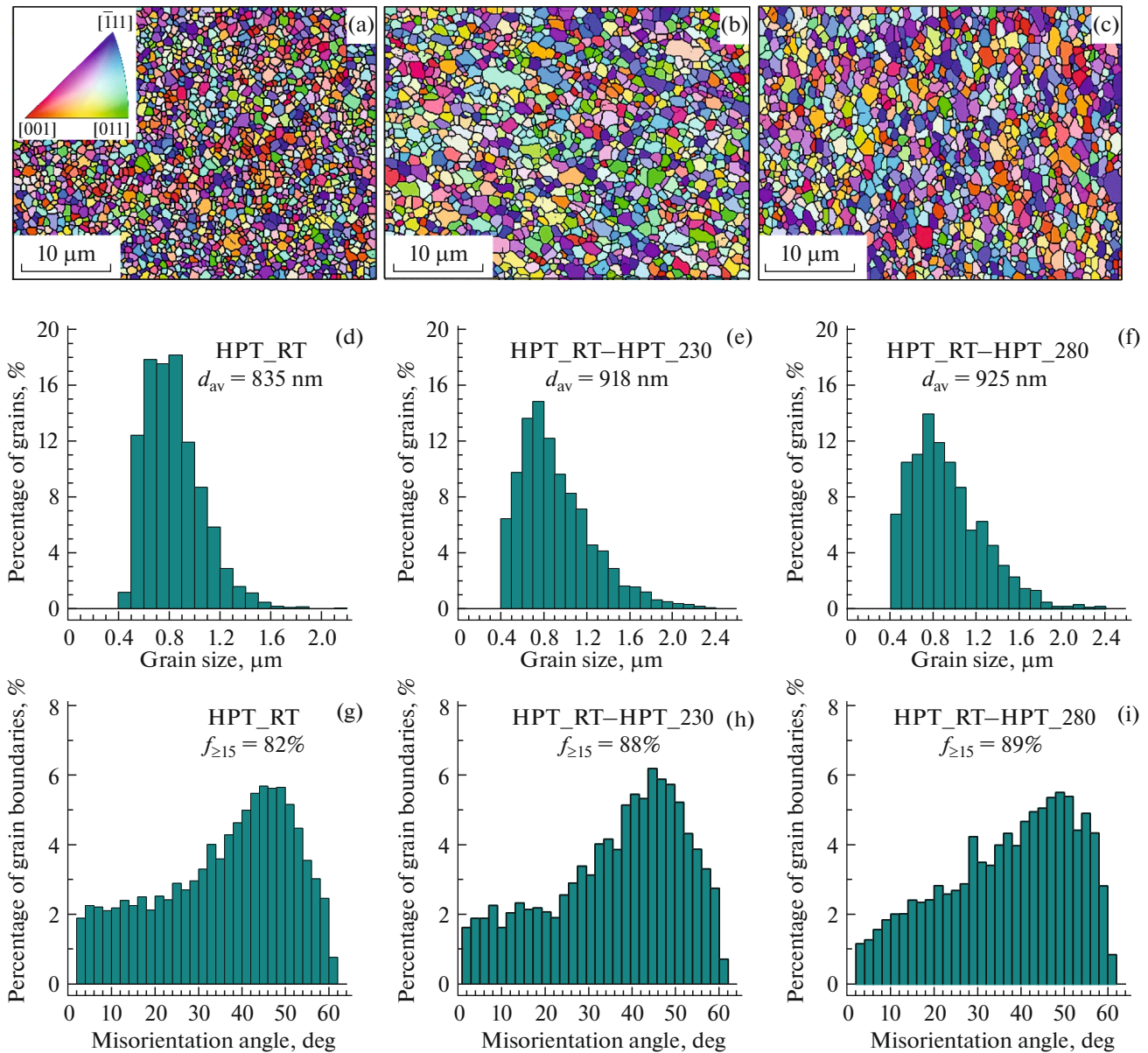
### 3.2. Evolution of the Microstructure

Figure 2 shows the EBSD maps and the diagrams constructed on the basis of their analysis for the grain size distribution and the distribution of GBs according to misalignments for the Al–0.4Zr alloy in the HPT\_RT, HPT\_RT–HPT\_230, and HPT\_RT–HPT\_280 states. The results of microstructural studies are given in Table 1; moreover, Table 1 contains the data for the Al–0.4Zr alloy in the initial state (before the SPTD treatment), as well as in the states after SPTD and annealing at 230 and 280°C for comparison (the HPT\_RT–AN\_230 and HPT\_RT–AN\_280 states, the data of [9]). As was noted earlier [9, 20], the initial state of the Al–0.4Zr alloy is characterized by elongated subgrains with an average length of about 1800 nm and a width of about 1000 nm (the proportion of HAGBs is 25%) (Table 1). The SPTD treatment leads to the formation of a homogeneous UFG structure formed by equiaxed grains, the average size of which is about 835 nm, and the proportion of HAGBs reaches 82% (see Figs. 2a, 2d, and 2g, and Table 1). After additional SPTD at  $T_{HPT} = 230^\circ\text{C}$ , the average grain size was about 918 nm, and the proportion of HAGBs was about 88% (see Figs. 2b, 2e, and 2h, and Table 1). Approximately the same parameters of the microstructure ( $d_{av} \sim 925$  nm and  $f_{\geq 15} \sim 89\%$ ) were obtained after additional SPTD at  $T_{HPT} = 280^\circ\text{C}$  (see Figs. 2c, 2f, and 2i, and Table 1). Additional SPTD at a temperature of 230°C leads only to an insignificant increase in the average grain size and the fraction of HAGBs in comparison with annealing for 1 h at the same temperature (Table 1). It should be noted that the obtained grain size distributions and the distribution of grain boundaries with misalignment angles are qualitatively similar for the HPT\_RT–HPT\_230 (this study) and HPT\_RT–AN\_230 [9] samples.

Microstructure parameters, such as the lattice parameter  $a$ , the mean size  $D_{XRD}$  of coherent scattering domains (CSDs), the level of microdistortions  $\langle \epsilon^2 \rangle^{1/2}$ , and the dislocation density  $L_{dis}$ , which are given in Table 1, were determined for the Al–0.4Zr alloy by an X-ray diffraction analysis. Owing to the prelimi-

nary SPTD treatment at RT, the formation of the UFG structure is accompanied by a noticeable decrease in the mean size of CSDs and an increase in the  $\langle \epsilon^2 \rangle^{1/2}$  level, from which an approximately two-fold increase in the  $L_{dis}$  value followed, according to formula (1). In addition to an increase in the average size of grains, the additional SPTD treatment at temperatures of 230 and 280°C leads to a significant increase in the CSD size and a decrease in the  $\langle \epsilon^2 \rangle^{1/2}$  values to the values typical of the initial state. Moreover, the  $L_{dis}$  values decrease by factors of about 4 and 7.5 times, respectively (Table 1). The annealing of the UFG alloy at a temperature of 230°C causes an approximately five-fold decrease in the  $L_{dis}$  value [5] (Table 1). Thus, comparison of the experimental data (Table 1) shows that additional SPTD at 230°C less efficiently reduces the density of dislocations in an UFG material in comparison with annealing. The noted difference is explained by the fact that the process of deformation at elevated temperatures leads not only to the annihilation of dislocations, which usually occurs during annealing, but also to the formation of new ones.

Figure 3 shows typical images of the microstructure and diffraction patterns taken from a single grain by the TEM method for samples of the Al–0.4Zr alloy in the initial (Fig. 3a), HPT\_RT (Fig. 3b), HPT\_RT–HPT\_230 (Figs. 3c and 3d), HPT\_RT–HPT\_280 (Figs. 3e and 3f) states. Similarly to [9], the TEM study did not reveal the presence of nanoscale precipitates of the secondary phase containing Zr in the initial and HPT\_RT states. As was shown earlier, all Zr in the Al–0.4Zr alloy in the initial state is in the solid solution [10, 11]. Similarly to annealing at a temperature of 230°C, SPTD at 230°C leads to the formation of a small amount of unevenly distributed nanosized particles (Figs. 6d and 6f), which indicates a decrease in the concentration of dissolved Zr atoms in the Al solid solution. The number of precipitated particles increases with an increase in the  $T_{HPT}$  temperature to 280°C (Figs. 3e and 3f). This is also evidenced by the appearance of additional reflections from the metastable Al<sub>3</sub>Zr phase (L<sub>2</sub>) in the X-ray diffraction pattern (Fig. 3e). A quantitative assessment of the average size



**Fig. 2.** (a–c) EBSD maps, (d–f) the grain size distribution, and (g–i) the distribution of grain boundaries in accordance with misalignment angles for the Al–0.4Zr alloy in the (a, d, g) HPT\_RT, (b, e, h) HPT\_RT–HPT\_230, and (c, f, i) HPT\_RT–HPT\_280 states.

of the precipitated particles gave 18–19 nm for both the HPT\_RT–HPT\_230 and HPT\_RT–HPT\_280 states of the UFG alloy.

#### 4. MECHANICAL PROPERTIES AND ELECTRICAL CONDUCTIVITY

Figure 4 shows the variation of the microhardness of the HPT\_RT samples with temperature  $T_{HPT}$  during additional SPTD (results of this study) and with annealing temperature  $T_{AN}$  during annealing for 1 h (data from [9]).

Figure 5 shows the stress–elongation diagrams for samples of the Al–0.4Zr alloy in various states, namely, the initial, HPT\_RT, HPT\_RT–HPT\_230, and HPT\_RT–HPT\_280 states, and also for HPT\_RT samples after annealing for 1 h at 230°C (data from [9]) and 280°C (data from this study), i.e., for the HPT\_RT–AN\_230 and HPT\_RT–AN\_280 states, respectively. The values of yield strength  $\sigma_{0.2}$ , ultimate tensile strength  $\sigma_{UTS}$ , and failure strain  $\delta$  determined from the experimental diagrams are given in Table 2. As can be seen, SPTD at elevated temperatures, as well as additional annealing, leads to a signif-



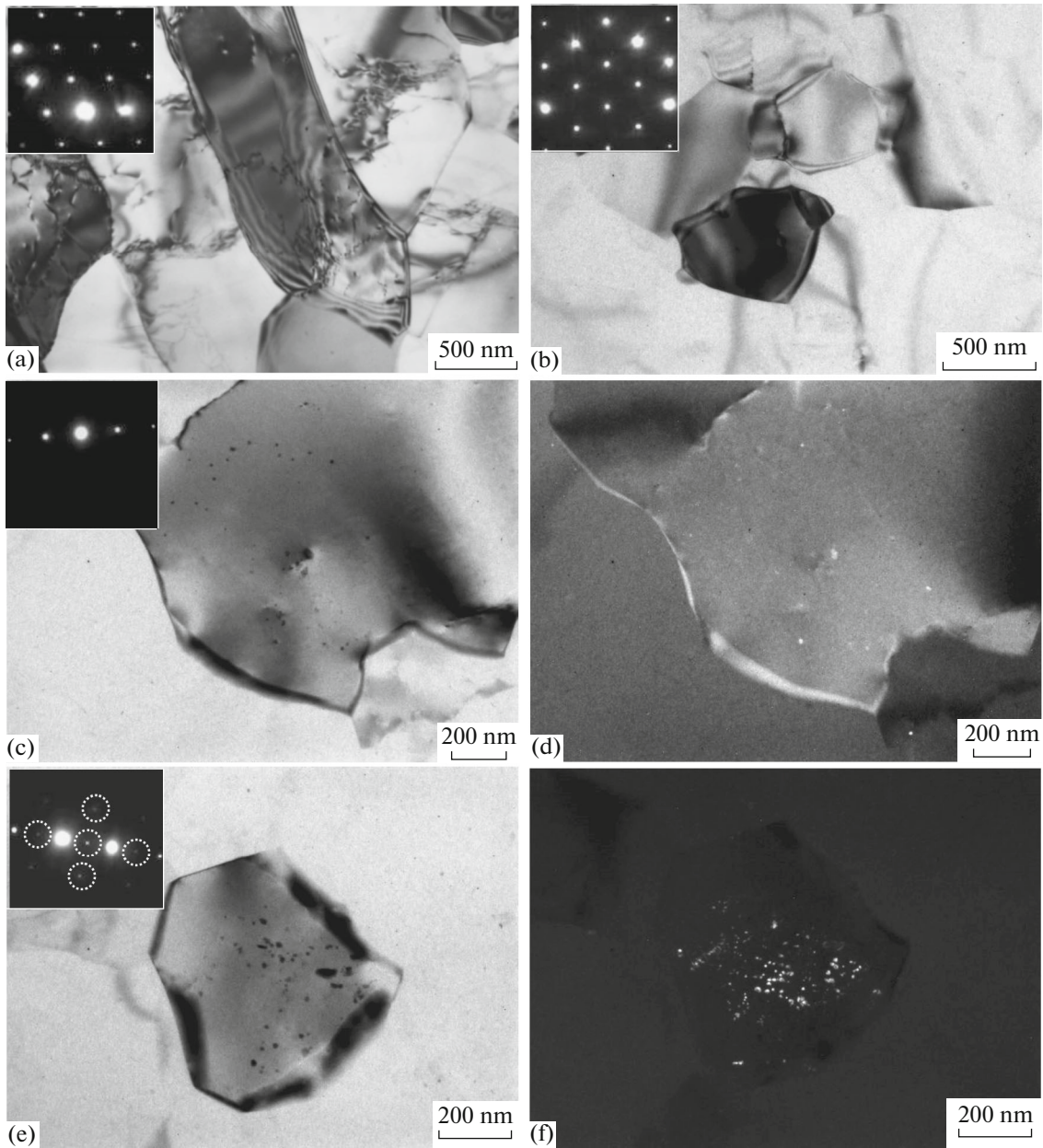


**Fig. 3.** TEM images with the corresponding diffraction patterns taken from a single grain for the Al–0.4Zr alloy in the (a) initial, (b) HPT\_RT, (c, d) HPT\_RT–HPT\_230, and (e, f) HPT\_RT–HPT\_280 states; the (a, b, c, e) bright-field and (d, f) dark-field images; (e) reflections from the secondary  $\text{Al}_3\text{Zr}$  phase in the diffraction pattern are marked by circles.

icant increase in the strength, and the  $H_V$ ,  $\sigma_{0.2}$ , and  $\sigma_{\text{UTS}}$  values obtained after additional deformation are even slightly higher than after annealing at the same temperatures. In addition, a small yield drop is observed on the tensile curves for the HPT\_RT–HPT\_230 and HPT\_RT–HPT\_280 states (Fig. 5).

The values of conductivity  $\sigma_{\text{RT}}$  for all studied states, i.e., the initial, HPT\_RT, HPT\_RT–HPT\_230 and HPT\_RT–HPT\_280 states, as well as the HPT\_RT–AN\_230 and HPT\_RT–AN\_280 states obtained in this study by the eddy-current method for compari-

son, are given in Table 2. A comparison of the variation of electrical resistivity  $\rho_{77}$  at 77 K with temperature  $T_{\text{HPT}}$  or  $T_{\text{AN}}$  for the UFG Al–0.4Zr alloy is shown in Fig. 6. As can be seen, the additional HPT treatment at elevated temperatures of 230 and 280°C leads to a significant increase in the electrical conductivity at RT and a decrease in  $\rho_{77}$  by 3.5 and 5.6 nΩ m, respectively. At the same time, the annealing at 230 and 280°C gives rise only to a small increase in  $\omega_{\text{RT}}$  and a decrease in  $\rho_{77}$  by 0.2 and 1.5 nΩ m, respectively. It should be noted that both the electrical conductivity

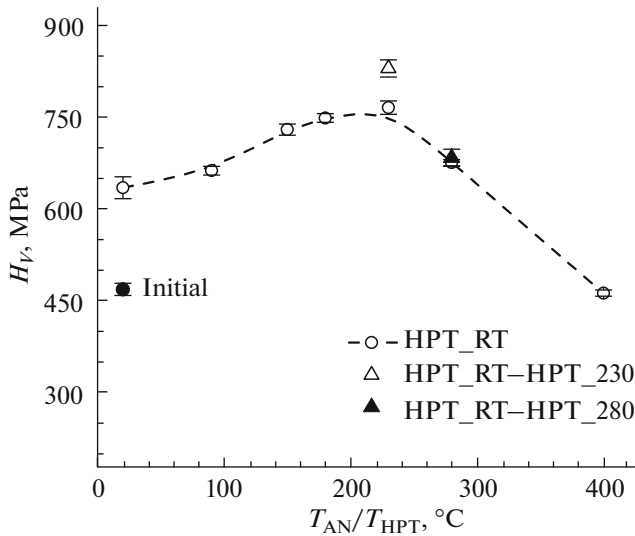


**Fig. 4.** Microhardness of the UFG Al–0.4Zr alloy (HPT\_RT) as a function of the temperature of the additional SPTD treatment at elevated temperatures (HPT\_RT–HPT\_230 and HPT\_RT–HPT\_280) (data obtained in this study) and the temperature of additional annealing (data published in [9]). The  $H_V$  value is also given for the initial state of the alloy.

and strength (microhardness) values practically remain the same with an increase in the duration of annealing at 230°C to 5 h (Table 2). Thus, both deformation and annealing of the UFG alloy at a temperature of 230°C lead to a significant increase in the

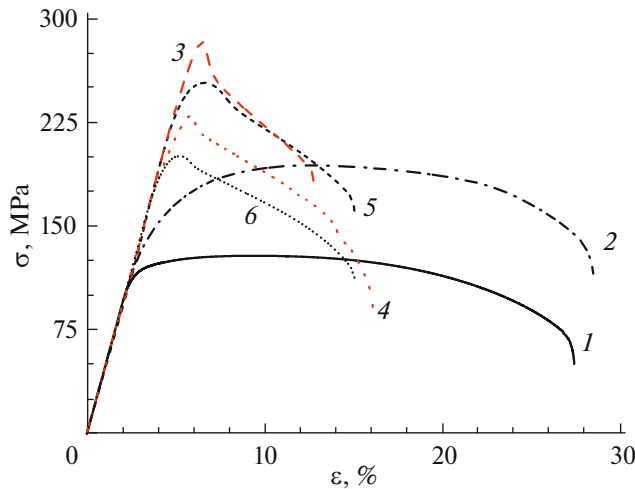


**Fig. 5.** Tensile diagrams for the Al–0.4Zr alloy in the initial state (curve 1), after SPTD at RT (curve 2), and after SPTD at RT and subsequent SPTD at elevated temperatures of 230 (curve 3) and 280°C (curve 4, data obtained in this study), as well as after the treatment of SPTD at RT and subsequent annealing for 1 h at 230°C (curve 5, data published in [9]) and 280°C (curve 6, data obtained in this study).

strength ( $\sigma_{0.2}$  and  $\sigma_{UTS}$ ) with a simultaneous increase in the electrical conductivity. However, additional SPTD at 230°C provides a much higher level of electrical conductivity (52% IACS) compared to annealing ( $\leq 49\%$  IACS) at the same temperature, even with an increase in its duration to 5 h, and also compared to annealing for 1 h at a higher temperature of 280°C (about 50% IACS) (Table 2).

5. DISCUSSION OF EXPERIMENTAL RESULTS

The maximum strengthening for the UFG Al–0.4Zr alloy after SPTD at elevated temperature, as well as after annealing, was achieved at  $T_{HPT}/T_{AN} = 230^\circ\text{C}$ . It is worth noting that the strengthening in both cases was accompanied by noticeable improvement in the electrical conductivity. Therefore, we analyze the change in the strength and electrical conductivity versus microstructural changes for the HPT\_RT–HPT\_230 state in comparison with those for the HPT\_RT–AN\_230 state.

Additional SPTD at 230°C led to a significant decrease in  $\rho_{77}^{\text{exp}}$  by about 3.5 nΩ m. According to Matthiessen’s rule [21], the contributions of various electron scattering mechanisms to the electrical resistance in metals and alloys in the temperature range of 77–300 K are summed:

$$\rho_{77}^{\text{th}} = \rho^{\text{pure}} + L_{\text{dis}}\Delta\rho^{\text{dis}} + S_{\text{GB}}\Delta\rho^{\text{GB}} + C_{\text{Zr}}^{\text{sol}}\Delta\rho_{\text{Zr}}^{\text{sol}} + \Delta\rho^{\text{pt}}, \tag{2}$$

where  $\rho^{\text{pure}} = 2.7 \text{ n}\Omega \text{ m}$  [22] is the resistivity of single-crystal aluminum;  $\Delta\rho^{\text{dis}} = 2.7 \times 10^{-25} \Omega \text{ m}^3$  [23] and

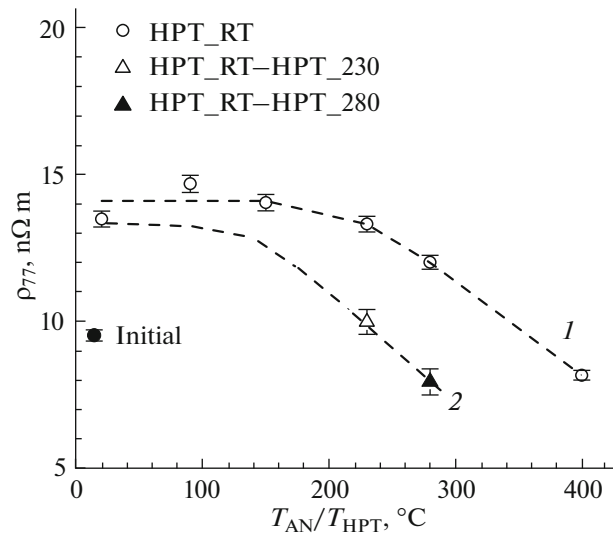


**Fig. 6.** Dependences of the resistivity at 77 K for the UFG Al–0.4Zr alloy (HPT\_RT) on the annealing temperature (curve 1, data published in [9]) or the temperature of the additional SPTD treatment (conditional curve 2, data obtained in this study).

**Table 2.** Mechanical and electrical properties of the Al–0.4Zr alloy in various states

Treatment	$H_v$ , MPa	$\sigma_{0.2}$ , MPa	$\sigma_{UTS}$ , MPa	$\delta$ , %	$\frac{\omega_{KT}}{\%IACS}$	$\rho_{77}$ , n $\Omega$ m	Ref.
Initial	470 $\pm$ 10	120 $\pm$ 2	130 $\pm$ 1	25.9 $\pm$ 0.2	49.1 $\pm$ 0.2	9.5 $\pm$ 0.2	[9]
HPT_RT	635 $\pm$ 18	140 $\pm$ 2	192 $\pm$ 2	23.2 $\pm$ 1	47.4 $\pm$ 0.1	13.5 $\pm$ 0.1	This study
HPT_RT–HPT_230	830 $\pm$ 14	265 $\pm$ 5	276 $\pm$ 7	7.7 $\pm$ 0.9	52.0 $\pm$ 0.4	10.0 $\pm$ 0.4	
HPT_RT–HPT_280	685 $\pm$ 14	230 $\pm$ 2	232 $\pm$ 2	15.7 $\pm$ 1	54.2 $\pm$ 0.7	7.9 $\pm$ 0.5	
HPT_RT–AN_230	765 $\pm$ 11	230 $\pm$ 2	250 $\pm$ 4	11.8 $\pm$ 0.4	48.7 $\pm$ 0.2*	13.3 $\pm$ 0.3	[9]
HPT_RT–AN_280	676 $\pm$ 5**	185 $\pm$ 3	203 $\pm$ 5	12.9 $\pm$ 0.5	50.3 $\pm$ 0.4	12.0 $\pm$ 0.6**	This study
HPT_RT–AN_230_5h	750 $\pm$ 10	–	–	–	48.1 $\pm$ 0.5	–	

\*Data obtained in this study; \*\*data published in [9].

$\Delta\rho^{GB} = 2.6 \times 10^{-16} \Omega \text{ m}^2$  [23] are the contributions from the specific density of dislocations and grain boundaries in Al, respectively;  $\Delta\rho_{Zr}^{sol} = 15.8 \text{ n}\Omega \text{ m/wt } \%$  [24] is the specific concentration of Zr in the solid solution;  $L_{dis}$  ( $\text{m}^{-2}$ ) is the density of dislocations;  $S_{GB}$  ( $\text{m}^{-1}$ ) is the bulk density of GBs;  $C_{Zr}^{sol}$  (wt %) is the concentration of Zr dissolved in the solid solution; and  $\Delta\rho^{pt}$  is the contribution from the particles of the secondary phase.

In a weakly doped Al–0.4Zr alloy, the maximum possible  $\Delta\rho^{pt}$  contribution to the electrical resistivity is negligible [9]. Estimates showed that changes in the dislocation density and grain size after SPTD at 230°C also give negligible changes in the contributions from dislocations (about  $7.3 \times 10^{-3} \text{ n}\Omega \text{ m}$ ) and from grain boundaries (about  $0.08 \text{ n}\Omega \text{ m}$ ), which is much smaller than an experimentally observed change of  $\Delta\rho_{77} \sim 3.5 \text{ n}\Omega \text{ m}$ . As in the case of annealing [9], the change in  $\rho_{77}$  after SPTD at a temperature of 230°C is mainly associated with a change in the concentration of Zr in the solid solution as a result of the formation of secondary phases. A change in the resistivity by  $3.5 \text{ n}\Omega \text{ m}$  indicates a decrease in the concentration of Zr in the solid solution by 0.22 wt %, which corresponds to the formation of  $\text{Al}_3\text{Zr}$  precipitates with a total volume of 0.27 vol %. It should be noted that SPTD at elevated temperature, when the DA process is activated in the UFG material, leads to a more effective (compared to annealing at the same temperature) decrease in the concentration of Zr in the solid solution due to the formation of nanosize precipitates of a secondary phase. Apparently, this is due to the fact that vacancies are more actively formed and annihilated during the SPTD process at higher temperatures, owing to additional deformation combined with thermal influence, which can accelerate diffusion processes that contribute to the nucleation and formation of secondary phases. In addition, dislocations in the SPTD process at elevated temperature, in contrast to the process of annealing, do not only annihilate but also are generated as main carriers of plastic deformation, which can

also contribute to the acceleration of diffusion. Deformation aging has led to a greater increase in the electrical conductivity compared to annealing at the same temperature of 230°C, owing to a more significant decrease in the concentration of Zr dissolved in the Al matrix, i.e., by 0.22 wt % for DA and by 0.008 wt % for annealing [9].

Usually, the general strengthening of metals and alloys is the sum of the contributions of various mechanisms to the general strengthening [25]:

$$\sigma_{0.2}^{th} = \sigma_0 + \sigma_{GB} + \sigma_{dis} + \sigma_{pt} + \sigma_{sol}, \quad (3)$$

where  $\sigma_0 = 10 \text{ MPa}$  is the Peierls–Nabarro stress of the crystal lattice of Al [26],  $\sigma_{GB}$  is the strengthening from grain boundaries,  $\sigma_{dis}$  is the strengthening from dislocations,  $\sigma_{pt}$  is the dopant strengthening from the particles of a secondary phase, and  $\sigma_{sol}$  is the solid solution strengthening.

The grain-boundary strengthening is determined by the Hall–Petch relation [27]:

$$\sigma_{GB} = Kd_{av}^{-1/2}, \quad (4)$$

where  $K = 0.07 \text{ MPa m}^{1/2}$  is the Hall–Petch coefficient [28], and  $d_{av}$  is the average grain size.

The contribution from the dislocation strengthening was estimated by the Taylor formula [29]:

$$\sigma_{dis} = M\alpha GbL_{dis}^{1/2}, \quad (5)$$

where  $M = 3.06$  is the Taylor factor [29],  $\alpha = 0.33$  is a parameter that takes into account the dislocation interaction [30],  $G = 26 \text{ GPa}$  is the shear modulus,  $b = 2.86 \text{ \AA}$  is the Burgers vector, and  $L_{dis}$  is the density of dislocations.

According to [31], the solid solution strengthening equals

$$\sigma_{sol} = \sum_i k_i C_i^{2/3}, \quad (6)$$

where  $C_i$  is the concentration of the  $i$ th dopant element, and  $k_{Zr} = 9 \text{ MPa/wt } \%^{2/3}$  is calculated according



**Table 3.** Results of estimation of the contributions of possible mechanisms to the overall strengthening of the Al–Zr alloy

State	$\sigma_0$ , MPa	$\sigma_{GB}$ , MPa	$\sigma_{sol}^*$ , MPa	$\sigma_{dis}$ , MPa	$\sigma_{Or}^{**}$ , MPa	$\sigma_{0.2}^{th}$ , MPa	$\sigma_{0.2}^{exp}$ , MPa	Ref.
Initial	10	59	5	28	0	102	120	This study
HPT_RT	10	77	5	45	0	137	140	"
HPT_RT–HPT_230	10	73	5	23	60	171	265	"
HPT_RT–AN_230	10	75	5	20	13	123	230	[9]

\*The maximum possible strengthening from the solid solution under conditions when all Zr is in the solid solution; \*\*the maximum possible Orowan strengthening.

to [32]. The obtained estimates of all contributions are given in Table 3.

In coarse-grained alloys, strengthening by particles of the secondary phase can be implemented in various ways: by cutting the particles, by enveloping them with dislocation loops (Orowan mechanism), or by a combination of these two mechanisms [33]. As was shown in [34], the Orowan mechanism operates in Al–Zr alloys with particles that are larger than 4.0 nm in diameter [33], which is expressed as

$$\Delta\sigma_{Or} = \frac{0.4MG_{Al}b}{\pi L\sqrt{I-v}} \ln\left(\frac{d_{av}\pi}{4b}\right), \quad (7)$$

where  $\nu = 0.345$  is Poisson's ratio for Al [35],  $\lambda$  is the distance between dopant particles calculated by the following equation [33]:

$$\lambda = \frac{d_{av}}{2} \left( \sqrt{\frac{2\pi}{3f_v}} - \pi \right), \quad (8)$$

where  $f_v$  is the volume fraction of precipitates of  $Al_3Zr$ .

It has been shown earlier that the Orowan strengthening is not realized in the UFG structure of the preaged Al–0.4Zr alloy, despite the formation of uniformly distributed nanosized (diameter about 13 nm) particles of the  $Al_3Zr$  phase [20, 36]. It should be noted that the amount of nanosized inclusions of the secondary phase in HPT\_RT–HPT\_230 is small and their distribution over the sample is inhomogeneous (Figs. 3c–3f); therefore, the Orowan strengthening, even if it is realized, cannot be significant. Estimates showed that the maximum contribution of the Orowan mechanism to the overall strengthening would not exceed 60 MPa in case it was realized under ideal conditions for a given UFG material (all particles of the secondary phase with a size of 18 nm were homogeneously distributed in the sample volume), whereas the resulting difference between  $\sigma_{0.2}^{th}$  and  $\sigma_{0.2}^{exp}$  (excluding strengthening from particles of the secondary phases) is 154 MPa for the HPT\_RT–HPT\_230 state (Table 3). In the case of annealing at 230°C, a significantly smaller number of particles with an approximately identical average size was observed, and the contribution to strengthening from them by the Orowan mechanism was estimated to be less than 20 MPa [9].

The experimental and theoretical  $\sigma_{0.2}$  values are in good agreement for the states before and after SPTD at RT (Table 3). However, for the UFG states after SPTD at 230°C, experimental values  $\sigma_{0.2}^{exp}$  significantly (almost by 100 MPa) exceed the obtained estimates of  $\sigma_{0.2}^{exp}$  (Table 3, Fig. 7) even with consideration of the maximum possible contribution from strengthening by the Orowan mechanism. A similar excess of  $\sigma_{0.2}^{exp}$  in comparison with theoretical estimates of  $\sigma_{0.2}^{exp}$  is also characteristic of the case of annealing at the same temperature (Table 3, Fig. 7) [9].

Thus, the results of the performed analysis indicate the operation of an additional strengthening mechanism caused by microstructural changes in the UFG Al–0.4Zr alloy as a result of SPTD at elevated temperatures or annealing at the same temperature. It is noteworthy that in spite of a substantially larger

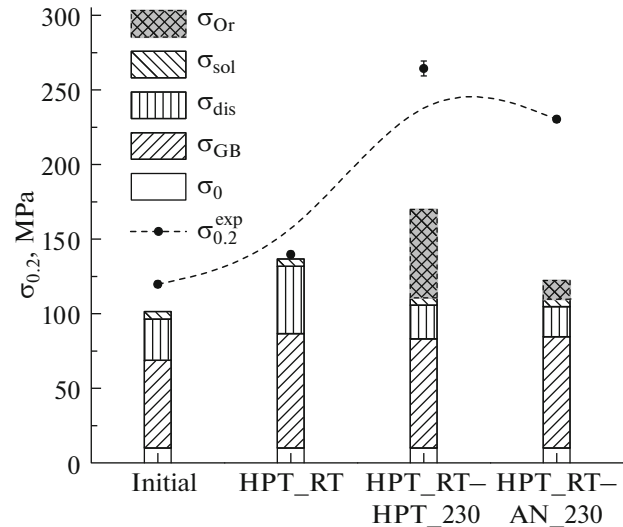


**Fig. 7.** Estimates of the contributions of possible mechanisms to the strengthening in comparison with experimentally obtained values of the conditional yield strength for the Al–0.4Zr alloy in the initial state and in the UFG states after SPTD at RT (HPT\_RT), after SPTD at RT and subsequent SPTD at 230°C (HPT\_RT–HPT\_230) (data obtained in this study) and after SPTD at RT and subsequent annealing at 230°C (HPT\_RT–AN\_230) [9].

amount of produced precipitates and, consequently, a more significant decrease in the concentration of zirconium in the solid solution in the case of implementation of SPTD at elevated temperature compared to annealing, the levels of strengthening ( $\sigma_{0.2}$  and  $\sigma_{UTS}$ ) of the UFG alloy hardly differ. The absence of a significant difference also indirectly indicates that strengthening after annealing or SPTD at elevated temperature is not due to the implementation of the Orowan mechanism. The observed small increase in  $\sigma_{0.2}^{exp}$  as a result of SPTD at 230°C compared to annealing at  $T_{AN} = 230^\circ\text{C}$  is mainly due to the appearance of a yield drop in the first case (Fig. 5).

Similarly to the case of annealing [9], it can be assumed that the additional strengthening of the UFG Al–Zr alloy as a result of deformation at elevated temperature is most likely caused by the relaxation of HAGBs [37–41], which may be accompanied by the formation of grain-boundary dopant segregations/nanoclusters/nanoprecipitates [41, 42]. Since it is known that SPTD at higher temperatures accelerates diffusion processes in UFG materials, the accelerated diffusion of dopant atoms can lead to the fixation of dislocations by them and to the appearance of a yield drop on stress–strain diagrams of the HPT\_RT–HPT\_230 and HPT\_RT–HPT\_280 samples (Fig. 5), as this was observed for a number of aluminum alloys (for example, in [13, 43]).

It is noteworthy that both annealing at 200°C and additional deformation at 200°C led to a significant decrease in  $\sigma_{0.2}$  and an almost two-fold decrease in  $\sigma_{UTS}$  for the UFG Al–2Fe (wt %) alloy, i.e., no effect of strengthening by annealing was observed in this system, although the UFG structure was also formed after SPTD under similar conditions [13]. The effect of strengthening was observed neither after additional SPTD at elevated temperatures [1] nor after annealing [6] also in alloys of the Al–Mg–Si system, in which the UFG structure was preliminarily formed by the SPTD method at RT. It should be noted that additional deformation at elevated temperatures in both of these systems led to the formation of nanosized particles of secondary phases. The electrical conductivity in these alloys, as in our material under study, increased owing to a marked decrease in the content of alloying elements in the solid solution; however, the strength of UFG alloys of the Al–Fe and Al–Mg–Si systems decreased significantly. The strength of these materials decreased during additional deformation at elevated temperature or during annealing mainly because of that the size of ultrafine grains increased significantly. In the Al–0.4Zr system, the grain size remains almost unchanged both after additional SPTD at elevated temperatures and after annealing [9], which indirectly indicates the effectiveness of fixing GBs and triple junctions by dopant segregations and/or nanoclusters/nanoprecipitates.

## 6. CONCLUSIONS

The effect of severe plastic torsion deformation at temperatures of 230 and 280°C on the microstructure, mechanical properties, and electrical conductivity of the UFG Al–0.4Zr alloy, the UFG structure of which was formed by the SPTD pretreatment at RT, is studied. It is shown that it is possible to simultaneously increase the strength characteristics ( $\sigma_{0.2}$  from 140 to 264 MPa and  $\sigma_{UTS}$  from 192 to 276 MPa) and electrical conductivity (from 49 to 52% IACS) by a factor of more than 1.5 after the additional SPTD of the UFG alloy at a temperature of 230°C.

The revealed tendency in the change of properties (strength and electrical conductivity) has also been observed earlier in this UFG alloy after additional annealing at the same temperature [9]. However, deformation at elevated temperatures leads to a more noticeable improvement in the properties of the UFG alloy compared to conventional annealing. Namely, the additional SPTD at temperatures of  $T_{HPT} = 230\text{--}280^\circ\text{C}$  ensures simultaneous increases in the strength to  $\sigma_{UTS} = 230\text{--}280$  MPa and in the electrical conductivity to 52–54% IACS, while a strength of  $\sigma_{UTS} = 200\text{--}250$  MPa with a conductivity level of 48.7–50.0% IACS is achieved after annealing for 1 h at  $T_{AN} = 230\text{--}280^\circ\text{C}$ . As in the case of annealing, the maximum strengthening due to the additional SPTD processing is achieved at  $T_{HPT} = 230^\circ\text{C}$ .

It is established that deformation aging, which occurs with additional deformation by the SPTD method at a temperature of 230°C, leads to the formation of a larger volume fraction of nanosized particles of the metastable  $\text{Al}_3\text{Zr}$  phase in comparison with annealing at a similar or even higher temperature (280°C) and, consequently, to a more significant decrease in the concentration of Zr in the solid solution of UFG aluminum, which gives rise to a significant increase in the electrical conductivity.

It is shown that a slight increase in the grain size and decreases in the density of dislocations and in the concentration of Zr in the solid solution are observed in the UFG alloy after the additional SPTD at elevated temperatures, which should lead to softening, whereas a nonstandard pattern of changing the strength, i.e., significant strengthening, is experimentally detected.

Assessments of the possible strengthening as a result of the formation of nanoscale precipitates of the  $\text{Al}_3\text{Zr}$  secondary phase because of dynamic aging with SPTD at  $T_{HPT} = 230^\circ\text{C}$  show that the observed strengthening cannot be explained by dispersion strengthening from these precipitates. The relaxation of nonequilibrium grain boundaries and the formation, along with intragranular particles of the  $\text{Al}_3\text{Zr}$  metastable phase, grain boundary segregations and/or nanoclusters/nanoprecipitates may be possible reasons for the strengthening of the UFG Al–0.4Zr alloy

upon additional SPTD at elevated temperatures, as well as upon annealing.

#### CONFLICT OF INTEREST

The authors declare that they have no conflicts of interest.

#### REFERENCES

- R. Z. Valiev, M. Yu. Murashkin, and I. Sabirov, *Scr. Mater.* **76**, 13 (2014).
- E. V. Bobruk, M. Yu. Murashkin, V. U. Kazykhanov, and R. Z. Valiev, *Rev. Adv. Mater. Sci.* **31**, 109 (2012).
- A. M. Mavlyutov, I. A. Kasatkin, M. Yu. Murashkin, R. Z. Valiev, and T. S. Orlova, *Phys. Solid State* **57**, 2051 (2015).
- R. Z. Valiev, A. P. Zhilyaev, and T. G. Langdon, *Bulk Nanostructured Materials: Fundamentals and Applications* (Wiley, Hoboken, 2013).
- I. Sabirov, M. Y. Murashkin, and R. Z. Valiev, *Mater. Sci. Eng. A* **560**, 1 (2013).
- X. Sauvage, E. V. Bobruk, M. Y. Murashkin, Y. Nasedkina, N. A. Enikeev, and R. Z. Valiev, *Acta Mater.* **98**, 355 (2015).
- T. Knych, M. Piwowarska, and P. Uliasz, *Arch. Met. Mater.* **56**, 685 (2011).
- D. I. Belyi, *Kabeli Provoda* **332**, 8 (2012).
- T. A. Latynina, A. M. Mavlyutov, M. Yu. Murashkin, R. Z. Valiev, and T. S. Orlova, *Philis. Mag.* (2019, in press).  
<https://doi.org/10.1080/14786435.2019.1631501>
- K. E. Knipping, D. C. Dunand, and D. N. Seidman, *Z. Metallk.* **97**, 246 (2006).
- N. A. Belov, A. N. Alabin, and A. R. Teleuova, *Met. Sci. Heat Treat.* **53**, 455 (2012).
- T. S. Orlova, A. M. Mavlyutov, A. S. Bondarenko, I. A. Kasatkin, M. Y. Murashkin, and R. Z. Valiev, *Philos. Mag.* **96**, 2429 (2016).
- A. E. Medvedev, M. Y. Murashkin, N. A. Enikeev, R. Z. Valiev, P. D. Hodgson, and R. Lapovok, *Adv. Eng. Mater.* **20**, 1700867 (2018).
- P. Ilario, US Patent No. 2659948 (1953).
- R. J. Schoerner, US Patent No. 3670401 (1972).
- R. Z. Valiev, R. K. Islamgaliev, and I. V. Alexandrov, *Prog. Mater. Sci.* **45**, 103 (2000).
- A. P. Zhilyaev and T. G. Langdon, *Prog. Mater. Sci.* **53**, 893 (2008).
- G. K. Williamson and R. E. Smallman, *Philos. Mag.* **1**, 34 (1956).
- F. J. Humphreys, *J. Microsc.* **195**, 170 (1999).
- A. M. Mavlyutov, T. A. Latynina, M. Yu. Murashkin, R. Z. Valiev, and T. S. Orlova, *Materialovedenie*, No. 3, 7 (2018).
- P. L. Rossiter, *The Electrical Resistivity of Metals and Alloys* (Cambridge Univ. Press, Cambridge, 2003).
- Properties and Selection: Nonferrous Alloys and Special-Purpose Materials*, *ASM Handbook* (ASM Int., 1990).
- A. S. Karolik and A. A. Luchvich, *J. Phys.: Condens. Matter* **6**, 873 (1994).
- F. Kutner and G. Lang, *Aluminum* **52**, 322 (1976).
- N. Kamikawa, X. Huang, N. Tsuji, and N. Hansen, *Acta Mater.* **57**, 4198 (2009).
- G. E. Totten and D. S. MacKenzie, *Handbook of Aluminium* (Marcel Dekker, New York, 2003).
- E. O. Hall, *Proc. Phys. Soc. B* **64**, 747 (1951).
- D. B. Witkin and E. J. Lavernia, *Prog. Mater. Sci.* **51**, 1 (2006).
- N. Hansen and X. Huang, *Acta Mater.* **46**, 1827 (1998).
- F. R. N. Nabarro, Z. S. Basinski, and D. B. Holt, *Adv. Phys.* **13**, 193 (1964).
- O. R. Myhr, O. Grong, and S. J. Andersen, *Acta Mater.* **49**, 65 (2001).
- K. E. Knipping, D. C. Dunand, and D. N. Seidman, *Acta Mater.* **56**, 114 (2008).
- W. Lefebvre, N. Masquelier, J. Houard, R. Patte, and H. Zapolsky, *Scr. Mater.* **70**, 43 (2014).
- C. B. Fuller, D. N. Seidman, and D. C. Dunand, *Acta Mater.* **51**, 4803 (2003).
- M. A. Meyers and K. K. Chawla, *Mechanical Metallurgy: Principles and Applications* (Paramus, NJ, Englewood Cliffs, 1984).
- T. S. Orlova, A. M. Mavlyutov, T. A. Latynina, E. V. Ubyivovk, M. Y. Murashkin, R. Schneider, D. Gerthsen, and R. Z. Valiev, *Rev. Adv. Mater. Sci.* **55**, 92 (2018).
- A. Hasnaoui, H. Van Swygenhoven, and P. M. Derlet, *Acta Mater.* **50**, 3927 (2002).
- A. M. Mavlyutov, T. A. Latynina, M. Yu. Murashkin, R. Z. Valiev, and T. S. Orlova, *Phys. Solid State* **59**, 1970 (2017).
- T. S. Orlova, N. V. Skiba, A. M. Mavlyutov, R. Z. Valiev, M. Y. Murashkin, and M. Y. Gutkin, *Rev. Adv. Mater. Sci.* **57**, 224 (2018).
- X. Huang, N. Hansen, and N. Tsuji, *Science* (Washington, DC, U. S.) **312**, 249 (2006).
- J. Hu, Y. N. Shi, X. Sauvage, G. Sha, and K. Lu, *Science* (Washington, DC, U. S.) **355**, 1292 (2017).
- Y. Zhang, Sh. J. P. Trimby, M. Y. Murashkin, R. Z. Valiev, and G. Sha, *Mater. Sci. Eng. A* **752**, 223 (2019).
- A. E. Medvedev, M. Y. Murashkin, N. A. Enikeev, I. Bikmukhametov, R. Z. Valiev, P. D. Hodgson, and R. Lapovok, *J. Alloys Compd.* **796**, 321 (2019).

Translated by O. Kadkin